Supporting Information

Exo- or Endo- 1*H*-Pyrazole Metal Coordination Modulated by Polyamine Chain length in [1+1] Condensation Azamacrocycles. Binuclear Complexes with Remarkable SOD activity.

Irene Bonastre-Sabater, Alberto Lopera, Álvaro Martínez-Camarena, Salvador Blasco, Antonio Doménech-Carbó, Hermas Jiménez, Begoña Verdejo, Enrique García-España, M. Paz Clares.

Contents

I. Figures

Figure S14. Experimental (top) and calculated (bottom) HR-ESI-Mass Spectra for the **[CuL3(ClO_4)]**$^+$ system, in H_2O/CH_3OH (50/50 vol/vol).

Figure S15. Experimental (top) and calculated (bottom) HR-ESI-Mass Spectra for the **[CuH$_{-1}$L1]**$^+$ system, in H_2O/CH_3OH (50/50 vol/vol).

Figure S16. Experimental (top) and calculated (bottom) HR-ESI-Mass Spectra for the **[CuH$_{-1}$L3]**$^+$ system, in H_2O/CH_3OH (50/50 vol/vol).

Figure S17. Experimental (top) and calculated (bottom) HR-ESI-Mass Spectra for the **[Cu$_2$H$_{-1}$L2(Cl)]**$^{2+}$ system, in H_2O/CH_3OH (50/50 vol/vol).

Figure S18. Experimental (top) and calculated (bottom) HR-ESI-Mass Spectra for the **[Cu$_2$H$_{-1}$L3(Cl)]**$^{2+}$ system, in H_2O/CH_3OH (50/50 vol/vol).

Figure S19. Experimental (top) and calculated (bottom) HR-ESI-Mass Spectra for the **[Cu$_2$H$_{-1}$L2(ClO_4)]**$^{2+}$ system, in H_2O/CH_3OH (50/50 vol/vol).

Figure S20. Experimental (top) and calculated (bottom) HR-ESI-Mass Spectra for the **[Cu$_2$H$_{-1}$L3(ClO_4)]**$^{2+}$ system, in H_2O/CH_3OH (50/50 vol/vol).

Figure S21. Experimental (top) and calculated (bottom) HR-ESI-Mass Spectra for the **[Cu$_2$H$_{-2}$L1]**$^{2+}$ system, in H_2O/CH_3OH (50/50 vol/vol).

Figure S22. Experimental (top) and calculated (bottom) HR-ESI-Mass Spectra for the **[Cu$_2$H$_{-2}$L2]**$^{2+}$ system, in H_2O/CH_3OH (50/50 vol/vol).

Figure S23. Experimental (top) and calculated (bottom) HR-ESI-Mass Spectra for the **[Cu$_2$H$_{-2}$L3]**$^{2+}$ system, in H_2O/CH_3OH (50/50 vol/vol).

Figure S24. Experimental (top) and calculated (bottom) HR-ESI-Mass Spectra for the **[Cu$_2$H$_{-2}$L1(Cl)]**$^+$ system, in H_2O/CH_3OH (50/50 vol/vol).

Figure S245. Experimental (top) and calculated (bottom) HR-ESI-Mass Spectra for the **[Cu$_2$H$_{-2}$L2(Cl)]**$^+$ system, in H_2O/CH_3OH (50/50 vol/vol).

Figure S26. Experimental (top) and calculated (bottom) HR-ESI-Mass Spectra for the **[Cu$_2$H$_{-2}$L3(Cl)]**$^+$ system, in H_2O/CH_3OH (50/50 vol/vol).

Figure S27. Experimental (top) and calculated (bottom) HR-ESI-Mass Spectra for the **[Cu$_2$H$_{-2}$L2(ClO_4)]**$^+$ system, in H_2O/CH_3OH (50/50 vol/vol).

Figure S28. Experimental (top) and calculated (bottom) HR-ESI-Mass Spectra for the **[Cu$_2$H$_{-2}$L3(ClO_4)]**$^+$ system, in H_2O/CH_3OH (50/50 vol/vol).

Figure S29. Paramagnetic ^{1}H NMR spectrum of the system Cu^{2+}–**L1** in a 2:1 molar ratio recorded in D_2O at pH=7.

Figure S30. Paramagnetic ^{1}H NMR spectrum of the system Cu^{2+}-**L3** for 2:1 molar ratio in D_2O at 298 K at pH=6.

Figure S31. ESR spectrum for the system Cu^{2+}–**L1**. [L] $1\cdot10^{-3}\cdot$M; = [Cu^{2+}] = $2\cdot10^{-3}$ M. H_2O. υ = 9.47 GHz. T = 77 K. pH 3, 6, 9 y 11.

Figure S32. ESR spectrum for the system Cu^{2+}-**L1**. [L] = [Cu^{2+}] = $1 \cdot 10^{-3}$ M compared to [L]= $1 \cdot 10^{-3}$ M, [Cu] = $2 \cdot 10^{-3}$ at different pH. H_2O. υ = 9.47 GHz. T = 77 K. pH 6, 9 y 11.

Figure S33. Cyclic voltammograms at the glassy carbon electrode of $1.0x10^{-3}$ M aqueous solutions for the mononuclear (a) Cu-**L2**, (b) Cu-**L3** and binuclear (b) Cu_2**L2,** (b)Cu-**L3** systems, in 0.15 M NaCl at pH 7.0. Potential scan initiated at 0.25 V vs. Ag/AgCl in the negative direction. Scan rate 50 mV/s.

Figure S34. ^{1}H NMR spectrum of **L1** in D_2O.

Figure S35. ^{13}C NMR spectrum of **L1** in D_2O.

II. Tables

Table S1. Chemical shift values, linewidths at half-height, transversal relaxation time values (T2) and assignments.

Table S2. The hyperfine-shifted resonances, linewidth and half-height and T2 values.

Table S3. Crystallographic data of crystal structures of complex **1** and **2**.

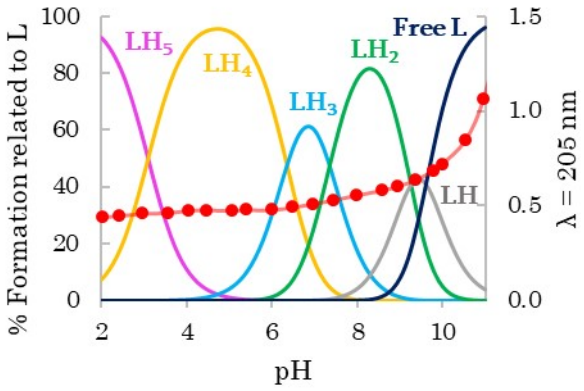

Figure S1. Distribution diagrams of the protonated species formed by **L1** overlapped with the absorbance at 205 nm

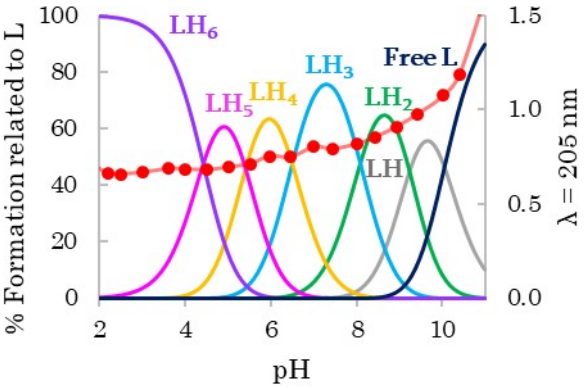

Figure S2. Distribution diagrams of the protonated species formed by **L2** overlapped with the absorbance at 205 nm

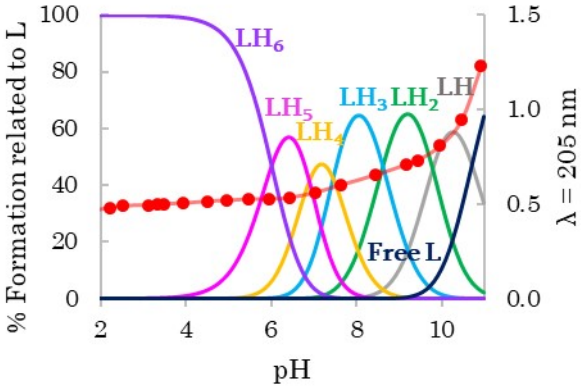

Figure S3. Distribution diagrams of the protonated species formed by **L3** overlapped with the absorbance at 205 nm

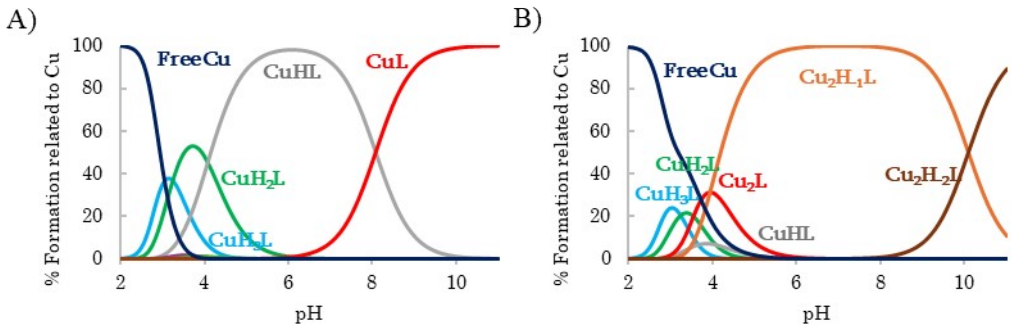

Figure S4. Distribution diagram for the system Cu^{2+}- **L2** molar ratio M:L 1:1 and 2:1

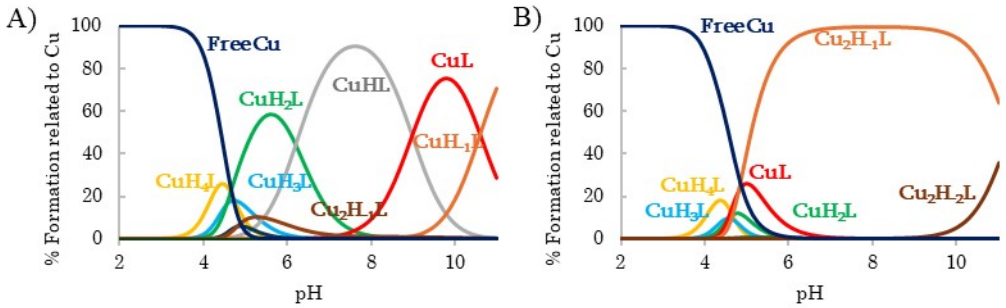

Figure S5. Distribution diagram for the system Cu^{2+}- **L3** molar ratio M:L 1:1 and 2:1

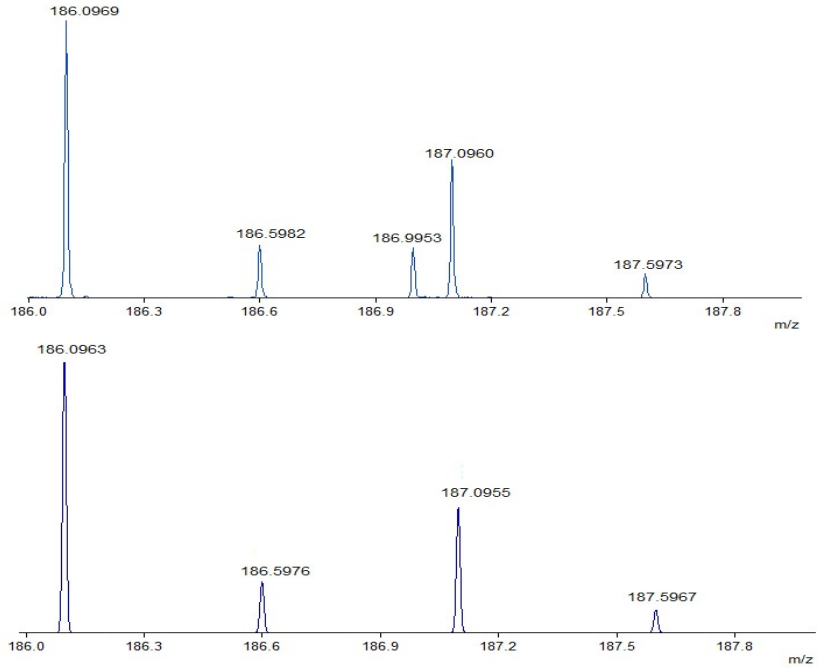

Figure S6. Experimental (top) and calculated (bottom) HR-ESI-Mass Spectra for the **$[CuL1]^{2+}$** system, in H_2O/CH_3OH (50/50 vol/vol).

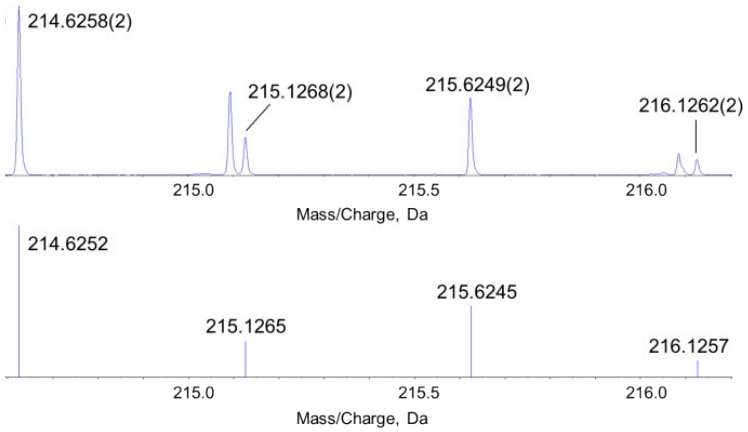

Figure S7. Experimental (top) and calculated (bottom) HR-ESI-Mass Spectra for the **[CuL2]**$^{2+}$ system, in H_2O/CH_3OH (50/50 vol/vol).

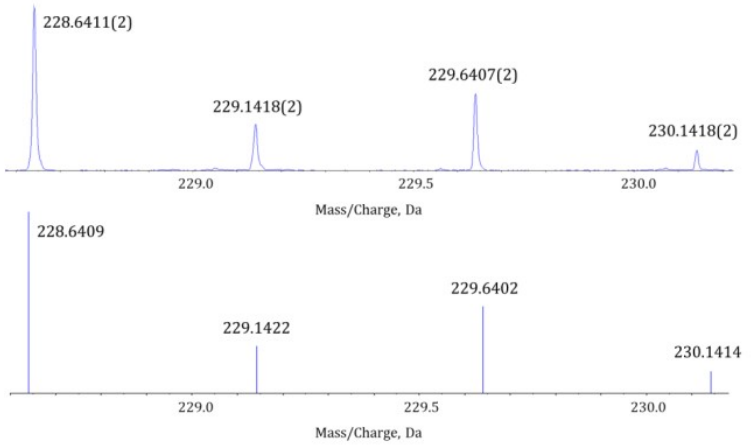

Figure S8. Experimental (top) and calculated (bottom) HR-ESI-Mass Spectra for the **[CuL3]**$^{2+}$ system, in H_2O/CH_3OH (50/50 vol/vol).

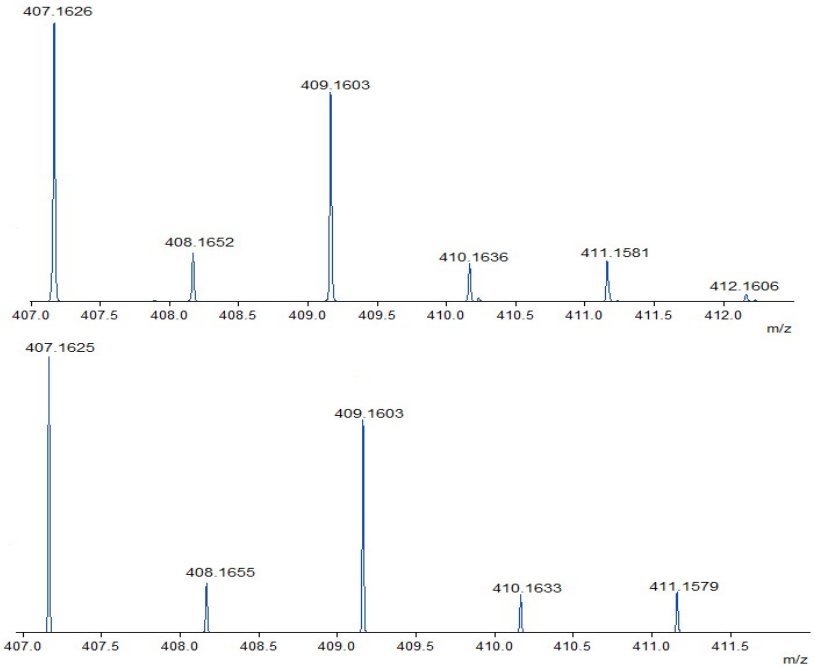

Figure S9. Experimental (top) and calculated (bottom) HR-ESI-Mass Spectra for the **[CuL1(Cl)]**$^+$ system, in H_2O/CH_3OH (50/50 vol/vol).

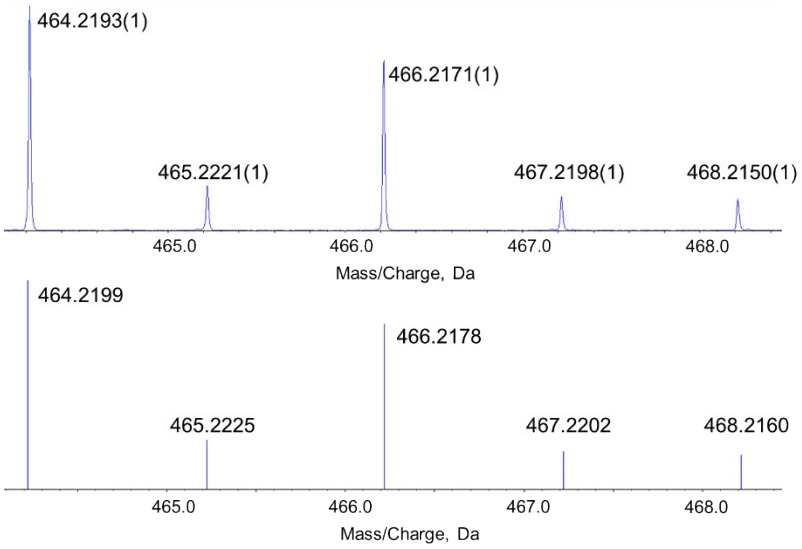

Figure S10. Experimental (top) and calculated (bottom) HR-ESI-Mass Spectra for the **[CuL2(Cl)]**$^+$ system, in H_2O/CH_3OH (50/50 vol/vol).

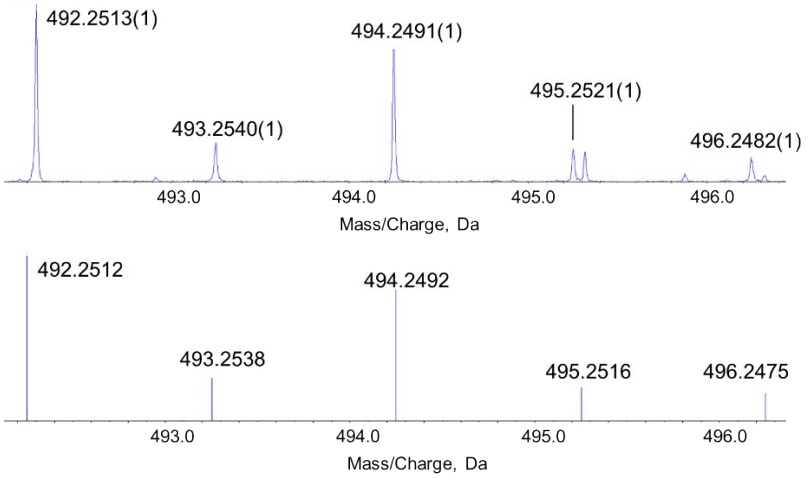

Figure S11. Experimental (top) and calculated (bottom) HR-ESI-Mass Spectra for the **[CuL3(Cl)]**$^+$ system, in H_2O/CH_3OH (50/50 vol/vol)

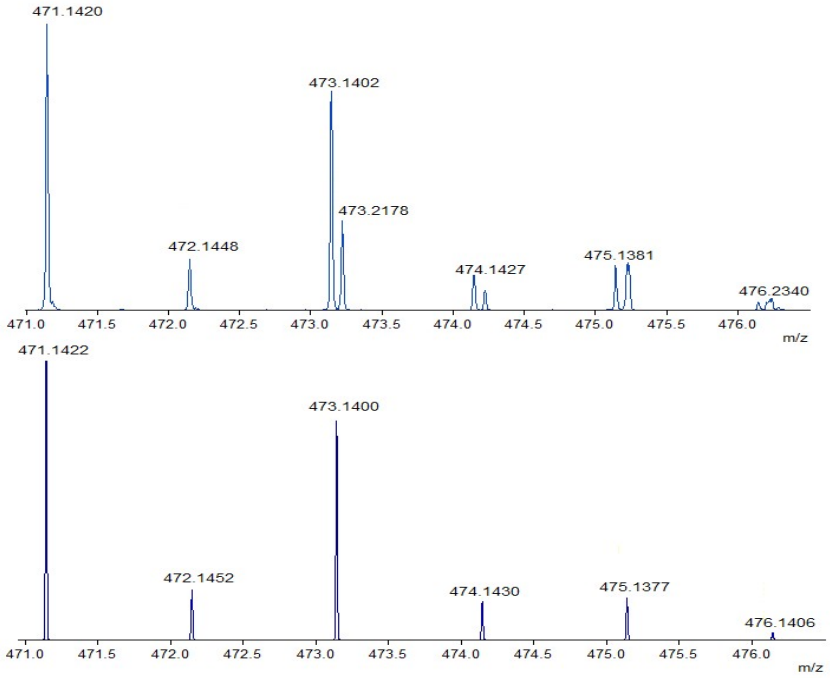

Figure S12. Experimental (top) and calculated (bottom) HR-ESI-Mass Spectra for the **[CuL1(ClO$_4$)]**$^+$ system, in H_2O/CH_3OH (50/50 vol/vol).

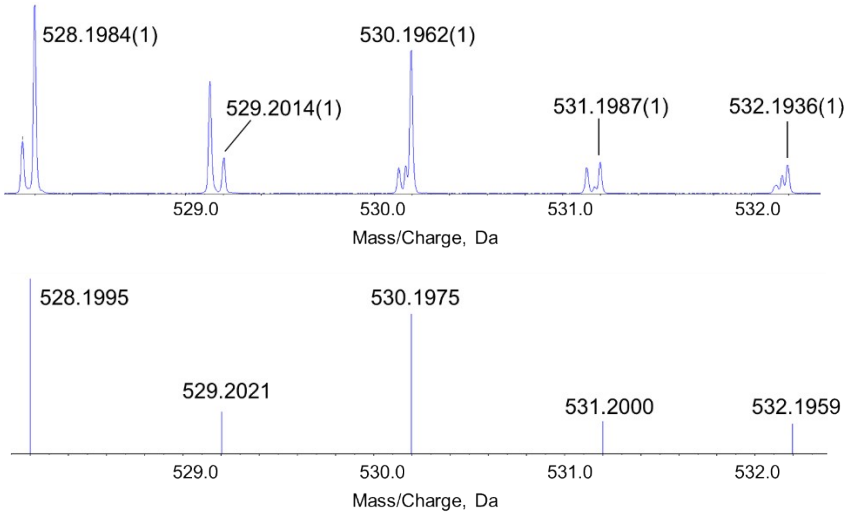

Figure S13. Experimental (top) and calculated (bottom) HR-ESI-Mass Spectra for the **[CuL2(ClO$_4$)]**$^+$ system, in H_2O/CH_3OH (50/50 vol/vol).

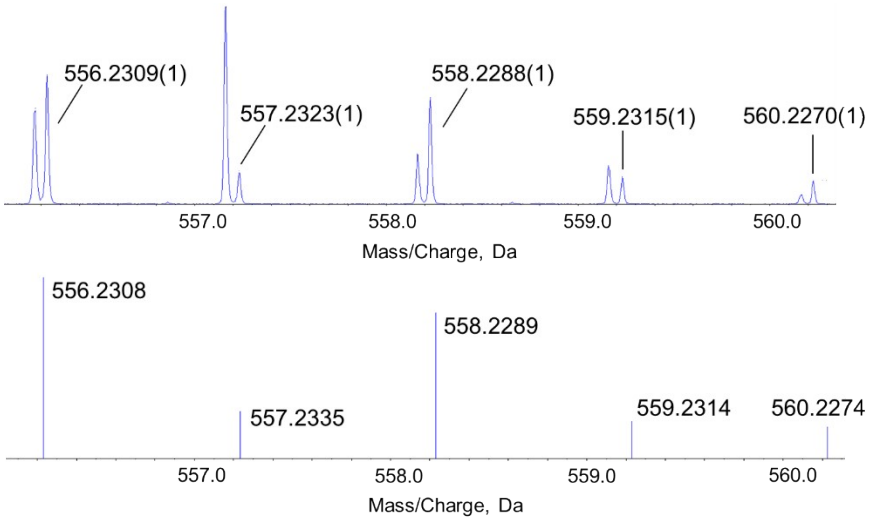

Figure S14. Experimental (top) and calculated (bottom) HR-ESI-Mass Spectra for the **[CuL3(ClO$_4$)]**$^+$ system, in H_2O/CH_3OH (50/50 vol/vol).

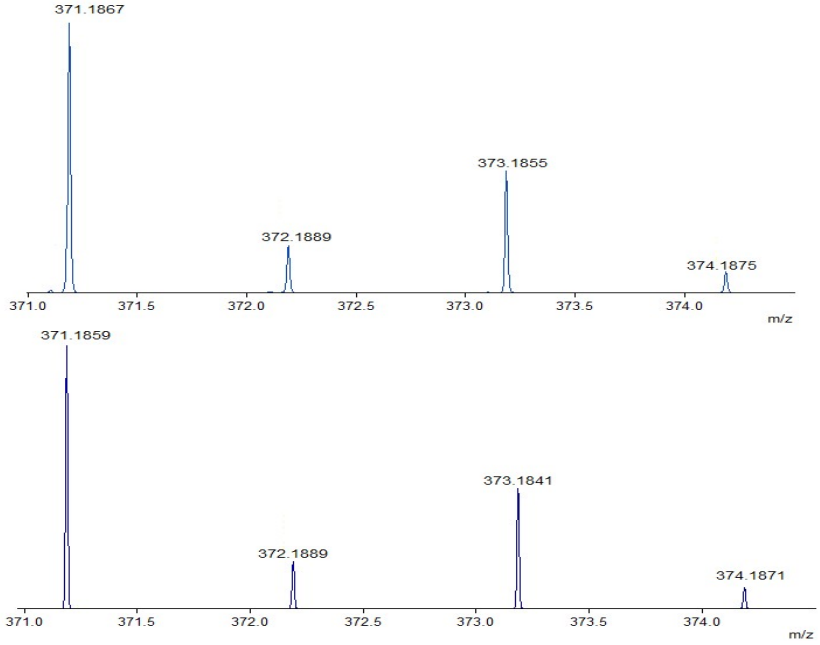

Figure S15. Experimental (top) and calculated (bottom) HR-ESI-Mass Spectra for the **[CuH$_{-1}$L1]**$^+$ system, in H_2O/CH_3OH (50/50 vol/vol).

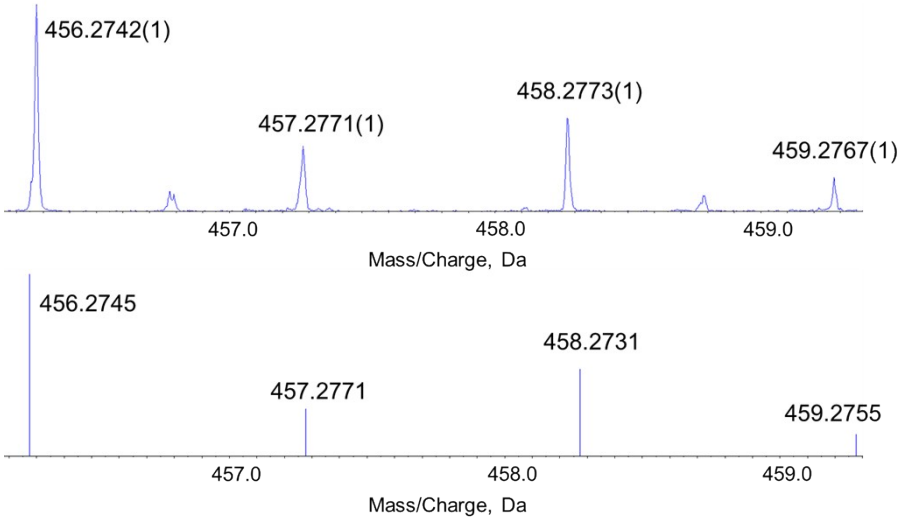

Figure S16. Experimental (top) and calculated (bottom) HR-ESI-Mass Spectra for the **[CuH$_{-1}$L3]$^{+}$** system, in H_2O/CH_3OH (50/50 vol/vol).

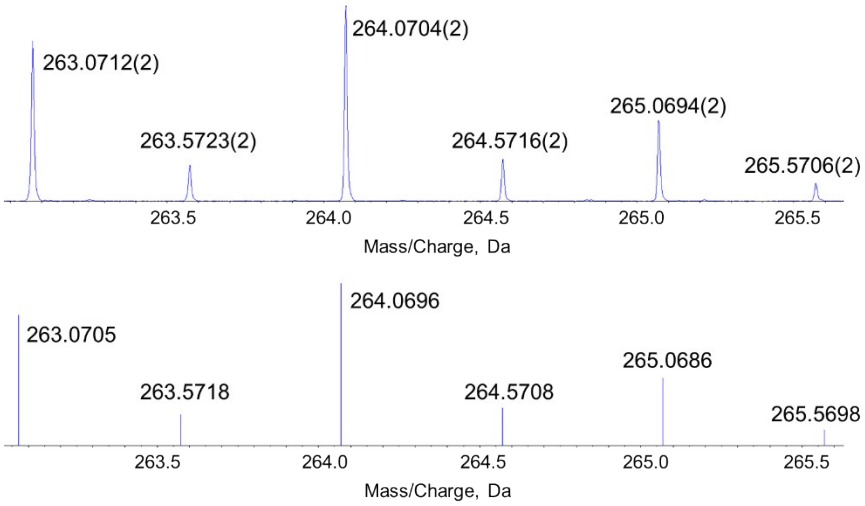

Figure S17. Experimental (top) and calculated (bottom) HR-ESI-Mass Spectra for the **[Cu$_2$H$_{-1}$L2(Cl)]$^{2+}$** system, in H_2O/CH_3OH (50/50 vol/vol).

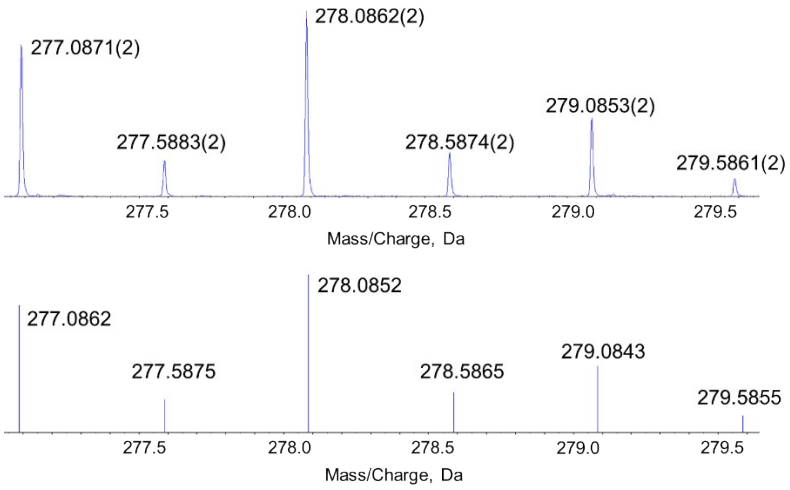

Figure S18. Experimental (top) and calculated (bottom) HR-ESI-Mass Spectra for the **[Cu$_2$H$_{-1}$**

$_1$**L3(Cl)]**$^{2+}$ system, in H_2O/CH_3OH (50/50 vol/vol).

Figure S19. Experimental (top) and calculated (bottom) HR-ESI-Mass Spectra for the **[Cu_2H_{-1}L2(ClO_4)]**$^{2+}$ system, in H_2O/CH_3OH (50/50 vol/vol).

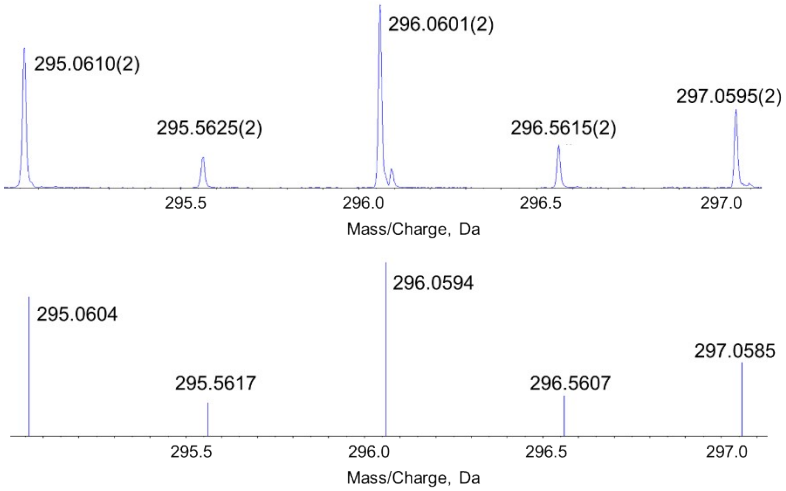

Figure S20. Experimental (top) and calculated (bottom) HR-ESI-Mass Spectra for the **[Cu_2H_{-1}L3(ClO_4)]**$^{2+}$ system, in H_2O/CH_3OH (50/50 vol/vol).

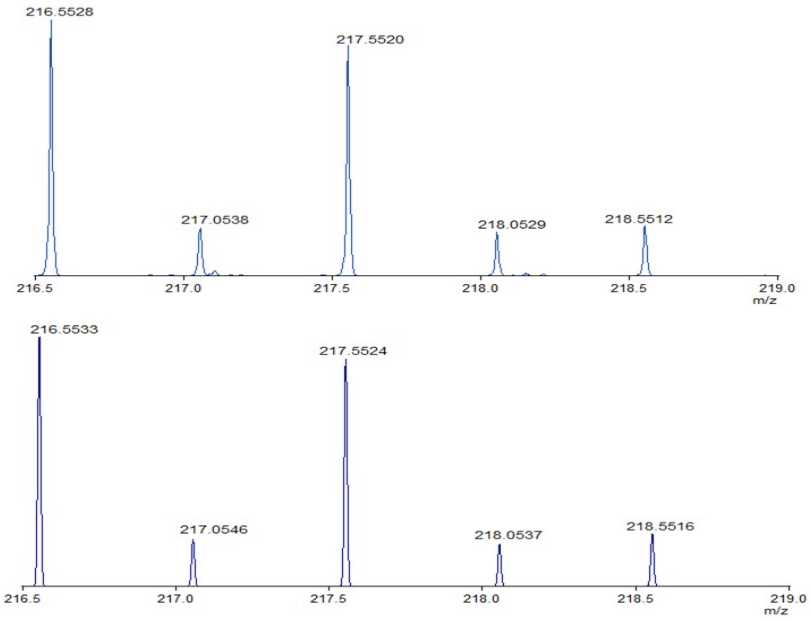

Figure S21. Experimental (top) and calculated (bottom) HR-ESI-Mass Spectra for the **$[Cu_2H_{-2}L1]^{2+}$** system, in H_2O/CH_3OH (50/50 vol/vol).

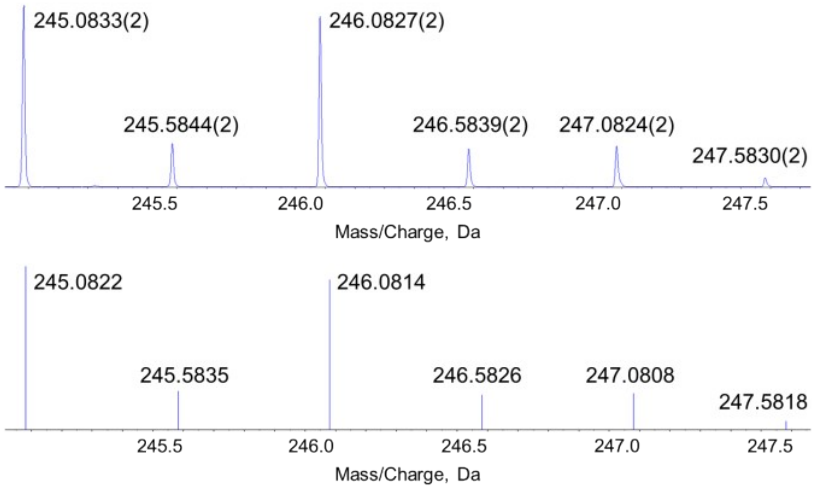

Figure S22. Experimental (top) and calculated (bottom) HR-ESI-Mass Spectra for the **$[Cu_2H_{-2}L2]^{2+}$** system, in H_2O/CH_3OH (50/50 vol/vol).

Figure S23. Experimental (top) and calculated (bottom) HR-ESI-Mass Spectra for the **$[Cu_2H_{-2}L3]^{2+}$** system, in H_2O/CH_3OH (50/50 vol/vol).

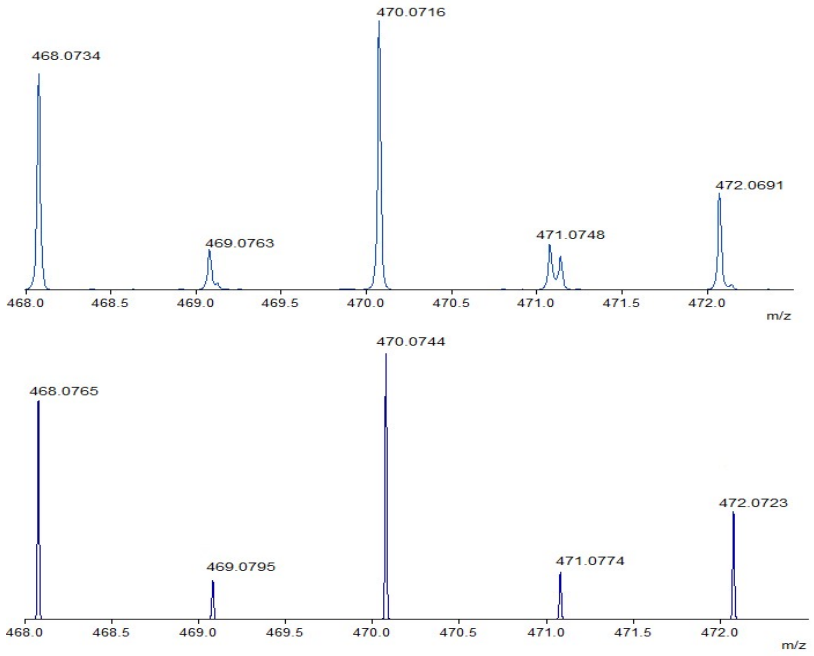

Figure S24. Experimental (top) and calculated (bottom) HR-ESI-Mass Spectra for the **$[Cu_2H_{-2}L1(Cl)]^{+}$** system, in H_2O/CH_3OH (50/50 vol/vol).

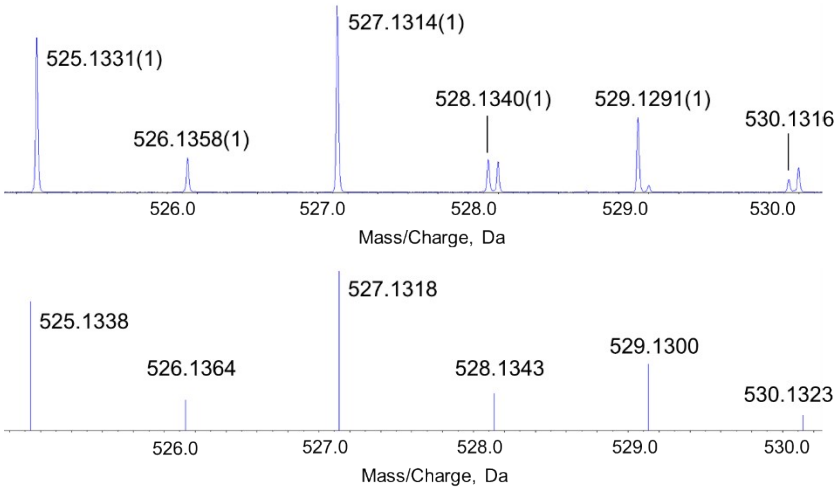

Figure S245. Experimental (top) and calculated (bottom) HR-ESI-Mass Spectra for the **[Cu_2H_2L2(Cl)]$^+$** system, in H_2O/CH_3OH (50/50 vol/vol).

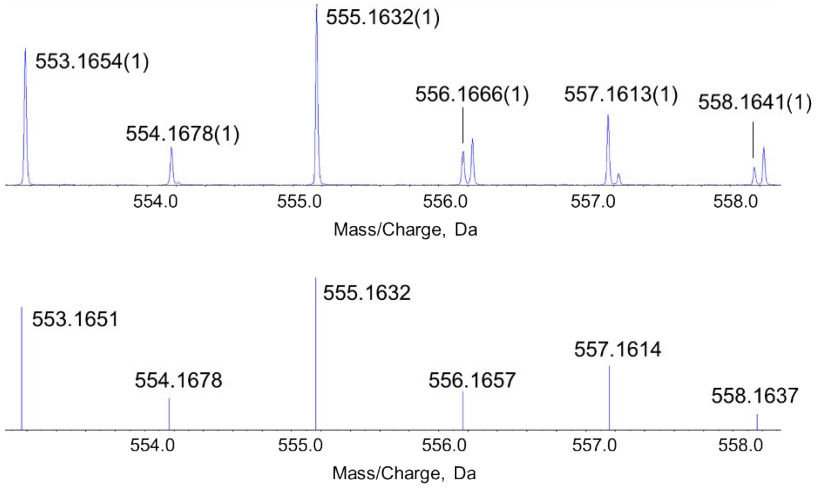

Figure S26. Experimental (top) and calculated (bottom) HR-ESI-Mass Spectra for the **[Cu_2H_2L3(Cl)]$^+$** system, in H_2O/CH_3OH (50/50 vol/vol).

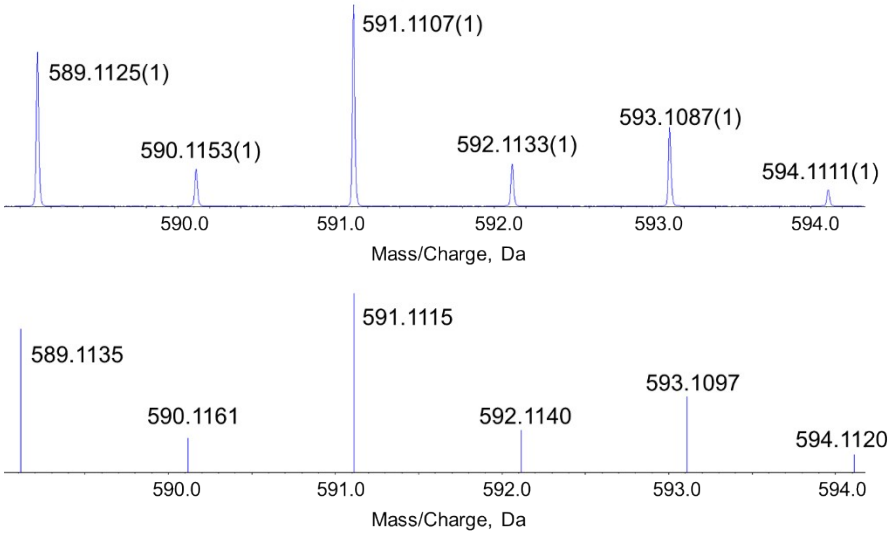

Figure S27. Experimental (top) and calculated (bottom) HR-ESI-Mass Spectra for the **[Cu_2H**

$_2$**L2(ClO$_4$)]**$^+$ system, in H_2O/CH_3OH (50/50 vol/vol).

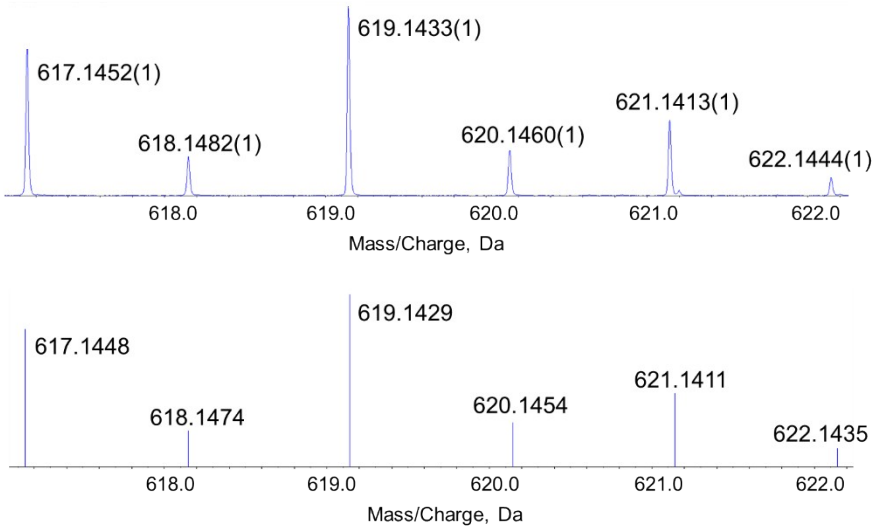

Figure S28. Experimental (top) and calculated (bottom) HR-ESI-Mass Spectra for the **[Cu$_2$H$_{-2}$L3(ClO$_4$)]**$^+$ system, in H_2O/CH_3OH (50/50 vol/vol).

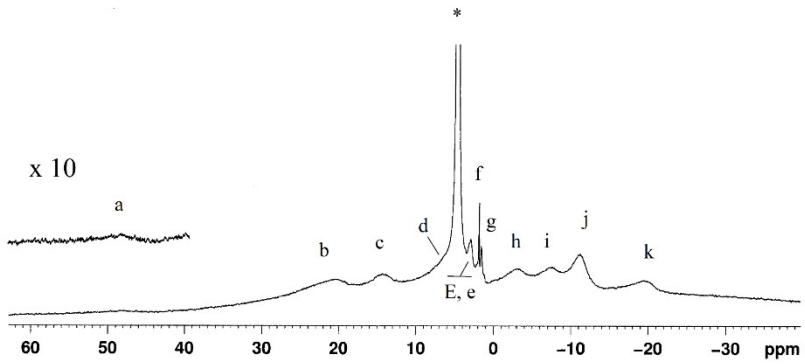

Figure S29. Paramagnetic ^{1}H NMR spectrum of the system Cu^{2+}–**L1** in a 2:1 molar ratio recorded in D_2O at pH=7

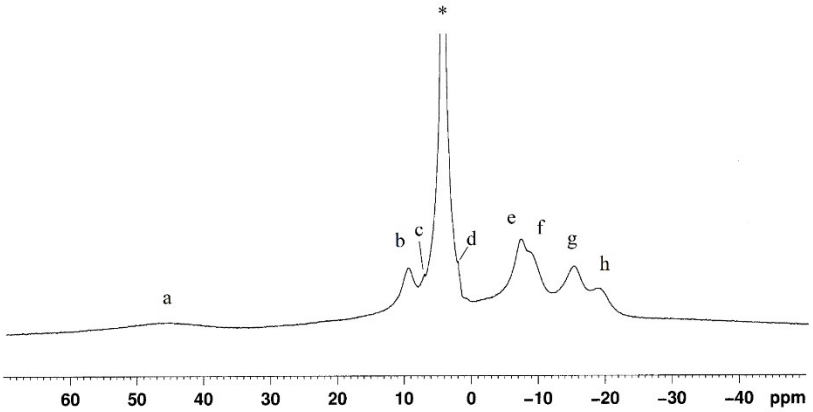

Figure S30. Paramagnetic ^{1}H NMR spectrum of the system Cu^{2+}-**L3** for 2:1 molar ratio in D_2O at 298 K at pH=6

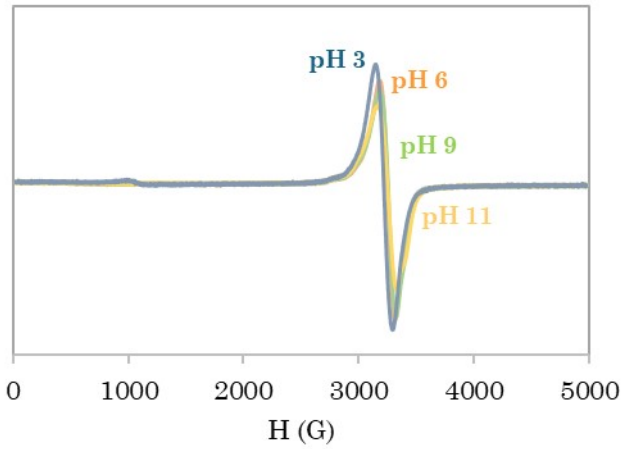

Figure S31. ESR spectrum for the system Cu^{2+}–**L1**. [L] $1\cdot10^{-3}\cdot$M; = [Cu^{2+}] = $2\cdot10^{-3}$ M. H_2O. υ = 9.47 GHz. T = 77 K. pH 3, 6, 9 y 11

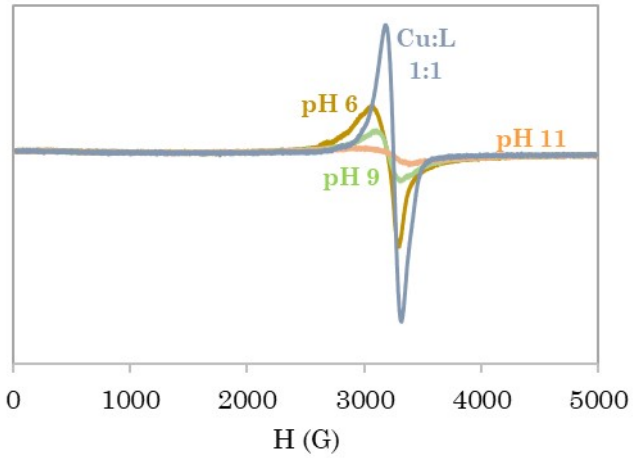

Figure S32. ESR spectrum for the system Cu^{2+}**-L1**. [L] = [Cu^{2+}] = $1\cdot10^{-3}$ M compared to [L]= $1\cdot10^{-3}$ M, [Cu] = $2\cdot10^{-3}$ at different pH. H_2O. υ = 9.47 GHz. T = 77 K. pH 6, 9 y 11.

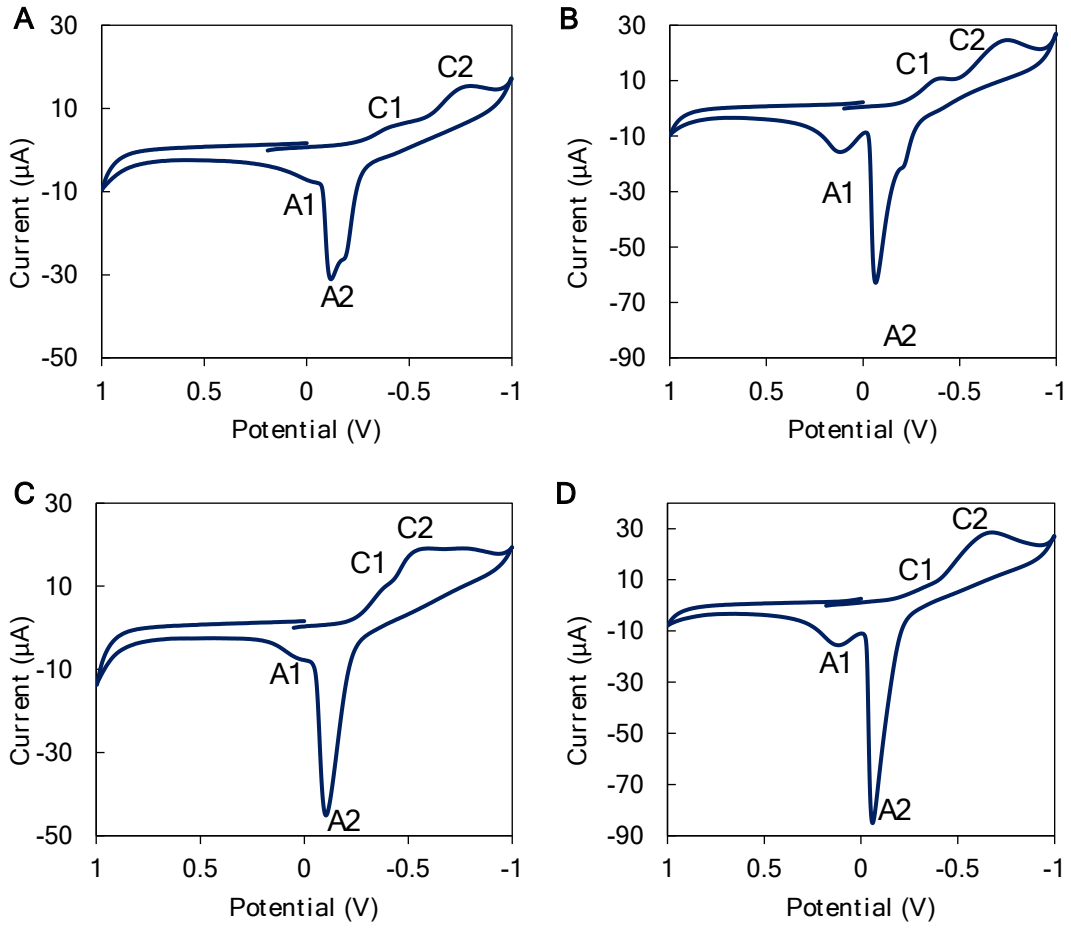

Figure S33. Cyclic voltammograms at the glassy carbon electrode of $1.0x10^{-3}$ M aqueous solutions for the mononuclear (a) Cu-**L2**, (b) Cu-**L3** and binuclear (b) Cu_2**L2,** (b)Cu-**L3** systems, in 0.15 M NaCl at pH 7.0. Potential scan initiated at 0.25 V vs. Ag/AgCl in the negative direction. Scan rate 50 mV/s

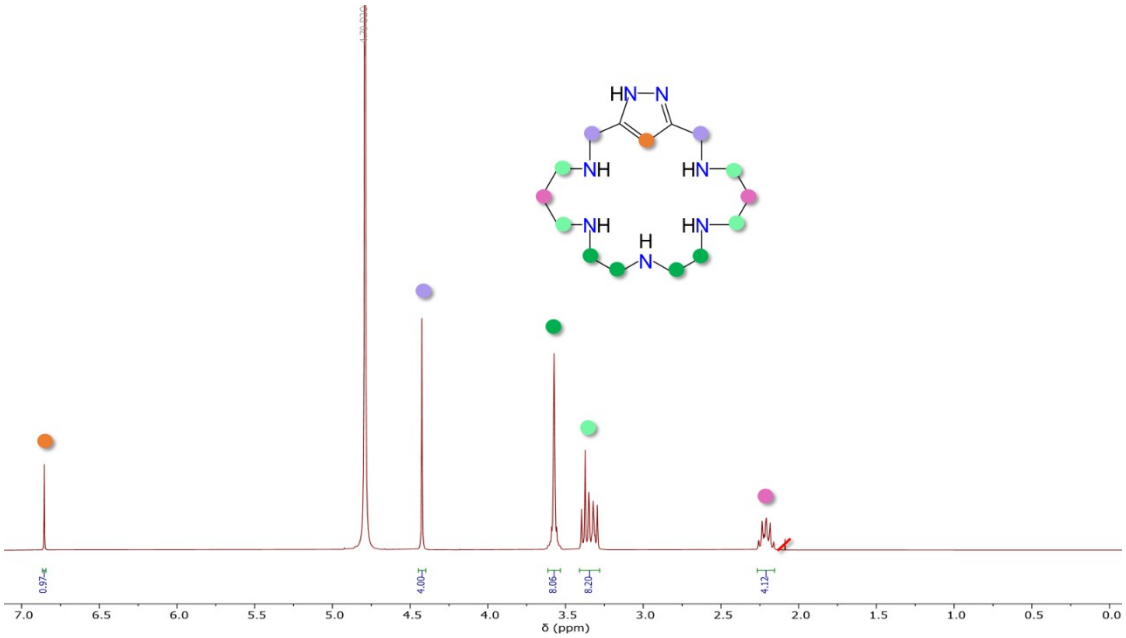

Figure S34. ^{1}H NMR spectrum of **L1**·6HBr in D_2O.

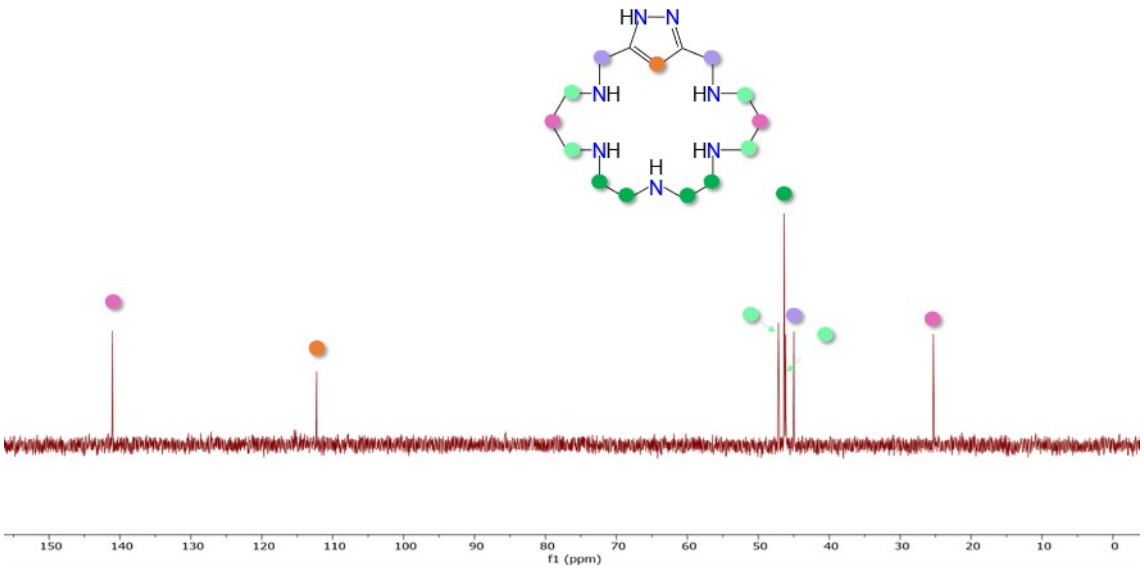

Figure S35. ^{13}C NMR spectrum of **L1**·6HBr in D_2O.

II. Tables

Table S1. ^{1}H NMR hyperfine-shifted resonances of Cu_2-**(L1)** complex in D_2O at 298 K and pH 7.

System	Signal	δ(ppm)	Nº of protons	Assignments	Temperature Dependence	$\Delta\nu_{1/2}$ (Hz)	T_2 [a] (ms)
Cu_2**(L1)**	a	48.0			Curie	2960	0.11
	b	20.6			Curie	1700	0.19
	c	14.4			Indep. of T	1178	0.27
	d	6.1	20	αCH_2	Curie	b	b
	h	-3.1			Curie	1006	0.32
	i	-7.4			Curie	850	0.37
	j	-11.2			Curie	1121	0.28
	k	-19.7			Curie	1811	0.18
	e	2.9			anti-Curie	b	b
	E[c]	3.0			Indep. of T	b	b
	f	1.9			anti-Curie	65	4.9
	g	1.6	5	βCH_2 H_m-Pz	anti-Curie	86	3.7

[a]Measured from the line width at half-height. [b]Overlap prevents measurement of this value.

[c]Measured at 313 K.

Table S2. ^{1}H NMR hyperfine-shifted resonances of Cu_2-**(L3)** complex in D_2O at 298 K and pH 6.

System	Signal	δ(ppm)	Nº of protons	Assignments	Temperature Dependence	$\Delta\nu_{1/2}$ (Hz)	T_2 [a] (ms)
Cu_2**(L3)**	a	46.5			Curie	4140	0.08
	b	9.8			Curie	1060	0.30
	e	-7.0			Curie	b	b
	f	-8.5			Curie	b	b
			24	αCH_2			
	g	-14.9			Curie	1044	0.31
	h	-18.6			Curie	b	b
	c	7.3			b	b	b
	d	2.5			b	b	b
			11	βCH_2, H_m-Pz			

[a]Measured from the line width at half-height. [b]Overlap prevents measurement of this value.

Table S3. Crystallographic data of crystal structures of complex **1** and **2**.

Structure	**1**	**2**
Composition	$C_{15}H_{33.75}Br_{2.87}Cl_{0.13}CuN_7O_{1.38}$	$C_{20}H_{45}Cl_3Cu_2N_8O_{10}$
Formula weight / g·mol^{-1}	631.94	791.07
Size / mm	0.202×0.126×0.075	0.253×0.172×0.146
Space group	P bca	P_{-1}
Unit cell		
• *a* / Å	14.263(4)	11.925(3)
• *b* / Å	14.560(4)	11.935(3)
• *c* / Å	21.837(6)	13.621(4)
• α / *degrees*	90	66.818(7)
• *β* / degrees	90	69.337(8)
• γ / degrees	90	65.348(12)
• *V* / Å^3	4535(2)	1577.8(7)
Density / g·cm^{-3}	1851	1,67
Z	8	2
μ / mm^{-1}	6.063	1.67
F000	2524	820
Diffraction Limits	$-23 \le h \le 23$	$-14 \le h \le 14$
	$-24 \le k \le 24$	$-14 \le k \le 14$
	$-36 \le l \le -28$	$-16 \le l \le 16$
R(int)	0.1048	0.0956
R(sigma)	0.0668	0.0623
Reflections		
• Total	110405	40075
• Unique	10964	5547
Parameters	321	421
Constraints	0	0
Restraints	24	14
*R*1		
• total	0.1100	0.1743
• $F^2 > 2\sigma(F^2)$	0.0459	0.1161
wR2		
• total	0.0994	0.2925
• $F^2 > 2\sigma(F^2)$	0.0773	0.2461
Goodnes of Fit	1.065	1.050
CCDC deposition	2240668	2215780